Morphology control of uniform $CaMoO_4$ based self-assembled microarchitectures and development of white light emitting phosphors by Ln doping (Ln= Dy^{3+}, Eu^{3+})

Mariano Laguna, Nuria O. Nuñez,*Ana I Becerro and Manuel Ocaña

Instituto de Ciencia de Materiales de Sevilla, CSIC, Américo Vespucio 49, 41092, Isla de la Cartuja, Sevilla, Spain

* corresponding author: nurianu@icmse.csic.es

Abstract

A very simple synthesis procedure based on precipitation reactions at moderated temperature (120ºC) from solutions containing calcium nitrate and sodium molybdate, using mixed solvents (polyols and water) has been developed which produces uniform tetragonal $CaMoO_4$ microarchitectures with different morphologies (peanuts, cocoons, spindles and spheres), which are composed by self-assembled entities. The morphology and crystal size of such assemblies could be tuned by a simple change of the nature of the components of the solvents mixture or their volumetric ratio in such mixture. All particles presented similar excitation and emission spectra arising from a charge transfer process within the MoO_4^{2-} groups. The emitted light presented a bluish-green color and its intensity was higher for the spindle-type particles. This synthesis procedure was also suitable for doping the peanut like $CaMoO_4$ architectures with Eu^{3+} or Dy^{3+} cations up to a 1% molar ratio (Ln/Ln+Ca), without altering their morphology or crystalline structure. The so prepared phosphors emitted an intense red (Eu-doped) or greenish (Dy-doped) light when excited through the MoO_4^{2-} groups excitation band indicating the presence of

an energy transfer process from such groups to the Ln^{3+} cations. Finally, a white light emitting phosphor with chromaticity coordinates x = 0.335 and y = 0.365, and a correlated color temperature of 5407 K was developed by codoping the peanut-type $CaMoO_4$ particles with proper amounts of Dy^{3+} (0.35%) and Eu^{3+} (0.15%) cations, which could find applications in white light emitting diodes.

1. Introduction

Lanthanide(Ln) based phosphors, usually consisting of a host matrix doped with active Ln^{3+}cations present several advantageous features when compared with other luminescent materials, which have favored their use for many technological applications in several fields ranging from optoelectronic (lasers, waveguides, plasma displays, LEDs, photovoltaics, photocatalysis, etc.),[1-5] to biotechnology (sensing, imaging, therapy, etc.).[6,7] These advantages include high chemical and thermal stability, photostability, high quantum yields, narrow emission bands and low toxicity, among others.[8] However, it must be also mentioned that the absorption coefficient of the Ln cations is low, which results in low intensity emissions.[9] To overcome this problem, several strategies can be adopted. One of them takes advantage of the large absorption coefficient of some inorganic anions, which are able to transfer the absorbed energy to the active Ln ions thus increasing the intensity of luminescence.[9] Among these anions are molybdates, which absorb UV light that can be transferred to some Ln^{3+} ions such as Eu^{3+}, Dy^{3+} or Tb^{3+}.[10] Because of this, a large variety of phosphors have been developed mostly based on different kinds of lanthanide[11] or alkaline earth[12-15] molybdates doped with Ln^{3+} cations.

It is also well known that the luminescent properties of Ln-based phosphors are affected by several factors, which include particle size and shape[16] for which, particles with uniform morphological features are usually required for most applications.

Among alkaline earth molybdates, calcium molybdate ($CaMoO_4$) is perhaps the most studied host matrix for the development of Ln-based phosphors. It must be mentioned that $CaMoO_4$ is itself luminescent because it emits blue light when excited with UV radiation.[17] The potential applications of this kind of phosphors encompass

biomedicine,[18] lighting,[10,13] and catalysis.[19] Up to now, several methods have been reported for the synthesis of $CaMoO_4$ microarchitectures with different shapes[20-27]. However, most of these methods conducted to particles with heterogeneous size and/or a certain degree of agglomeration, except in the case of the persimmon-like (2 μm)[20] particles obtained in a microwave reactor without temperature control and the spherical particles hydrothermally synthesized in the absence (5-6 μm)[22] or the presence (2 μm)[23] of a capping polymer (poly(diallyldimethyl-ammonium chloride).

Herein, we report on a very simple procedure for the synthesis of highly uniform $CaMoO_4$ microarchitectures consisting of self-assembled nanocrystals, based on precipitation reactions at moderated temperature from solutions containing calcium nitrate and sodium molybdate, using mixed solvents (polyols and water). Interestingly, the morphology (peanuts, cocoons, spindles, spheres) and crystallinity of such assemblies can be tuned by a simple change of the nature of the solvents used for the mixture or their volumetric ratio in such mixture. This effect is discussed in terms of the variations in viscosity and dielectric constant of the solvent. This procedure is also suitable for doping the $CaMoO_4$ architectures with Ln cations, which is first illustrated for the Eu^{3+} case, selected as a proof of concept to analyze the effect of doping on the morphological and structural features of the obtained red phosphors. Finally, white light emitting phosphors were obtained by doping the $CaMoO_4$ particles with proper amounts of Dy^{3+} cations. It is shown that the correlated color temperature of the white light so generated can be modulated by varying the Dy^{3+} doping level or by codoping with Eu^{3+} cations, which provides a red component thus resulting in a warmer white light.[28] These phosphors are of particular interest for developing white LEDs, since for this technology, single phase white light emitting phosphors are being proposed to minimize

the inhomogeneous temporal degradation of the systems based on the simultaneous emission of three different phosphors emitting red, green and blue light, respectively.[4]

2. Experimental

2.1. Reagents

Calcium nitrate ($Ca(NO_3)_2 \cdot 4H_2O$, Aldrich 99-103%), europium nitrate ($Eu(NO_3)_3 \cdot 5H_2O$, Aldrich, 99.9%), dysprosium nitrate ($Dy(NO_3)_3 \cdot xH_2O$, Aldrich, 99.9%) and sodium molybdate (Na_2MoO_4, Aldrich, ≥98%), were selected as precursors. Glycerol (GLY, Aldrich, ≥99.5%), ethylene glycol (EG, Aldrich, ≥99.5%) and mixtures GLY/H_2O and GLY/EG were used as solvents. All chemicals were used as received.

2.2. Nanoparticle synthesis

$CaMoO_4$ nanoparticles were prepared according to the following procedure. First, 0.02 mol dm^{-3} of $Ca(NO_3)_2$ and 0.1 mol dm^{-3} of Na_2MoO_4 were separately dissolved in 2.5 cm^3 of the desired solvent (GLY, EG, H_2O, GLY/H_2O or GLY/EG mixtures). To facilitate the dissolution of reagents in GLY and EG, the solutions were mildly heated (~ 80°C) under magnetic stirring. After cooling to room temperature, both solutions were mixed and magnetically stirred. The volumetric ratio of the GLY/H_2O and GLY/EG mixtures in the final solutions, was varied from 4/1 to 1.5/3.5, in order to investigate the effect of this parameter on the characteristics of the precipitated particles. Such solutions (total volume = 5 cm^3) were then aged for 20 hours in tightly closed test tubes using an oven preheated at 120°C. After aging, the resulting dispersions were cooled down to room temperature, centrifuged to remove the supernatants and washed, twice with ethanol and once with distilled water. Finally, the

precipitates were redispersed in milliQ water or, for some analyses, dried at room temperatures.

2.3. Ln-doped $CaMoO_4$ nanoparticles

To obtain Ln-doped $CaMoO_4$ phosphors we proceeded as described above for the case of pure $CaMoO_4$ system but incorporating the desired amount of the doping ion precursor (Eu, Dy or Eu/Dy) to the starting $Ca(NO_3)_2$ solution. The total cations concentration in these solutions was kept constant (0.02 mol dm^{-3}). The Ln/(Ln+Ca) molar ratio was varied in order to investigate the effects of the doping level on the morphology and luminescent properties of the precipitated nanoparticles.

2.4. Characterization

Particle shape was analized by scanning (FEGSEM, Hitachi S4800, 20 Kv) and transmission (TEM, Philips 200CM, 200 Kv) electron microscopy. For this, a droplet of an aqueous suspension of the sample was deposited on a copper grid coated with a transparent polymer and dried. Particle size was measured by counting several hundred of particles from the SEM and TEM micrographs using the free software *ImageJ*.

The qualitative composition of the precipitated particles was assessed by energy dispersive x-ray analysis (EDX, EDX Bruker X Flash Detector 4010) coupled to the SEM microscope. The infrared spectra (FTIR) of the powdered samples diluted in KBr pellets were recorded in a Fourier transform spectrometer (Jasco FT/IR-6200).

The crystalline structure of the prepared particles was identified by X-ray diffraction (XRD, Panalytical X´Pert Pro with an X-Celerator detector). Unit cell parameters were determined from the XRD data (collected at intervals of 0.02° (2θ) for an accumulation time of 1000 s) by Rietveld refinement using the X´Pert High Score Plus software. The

structural data for the $CaMoO_4$ phase was taken from Lee et al.[29] Refined parameters were: zero, background coefficients, scale factor and lattice parameters. The obtained Rwp values were in all cases in the 20-26% range. The crystallite size was estimated from the most intense XRD peak of the $CaMoO_4$ (112) (located at 28.7º 2θ) by using the Scherrer formula and LaB_6 as external standard.

The excitation and emission spectra of the samples dispersed in water (1 mg cm^{-3}) were recorded in a Horiba Jobin-Yvon Fluorolog3 spectrofluorometer operating in the front face mode. Lifetime measurements for Eu^{3+} and Dy^{3+} cations were obtained under pulsed excitation at λ_{exc} 532 nm and 355 nm, respectively, using the second and third harmonics of an Nd:YAG laser (Spectra Physics model DCR 2/2A 3378) with a pulse width of 10 ns and a repetition rate of 10 Hz. Fluorescence was analyzed through an ARC monochromator model SpectraPro 500-i and then detected synchronously with an EMI-9558QB photomultiplier and recorded by a Tektronix DPO4104B-L digital oscilloscope.

The CIE color coordinates were calculated from the emission spectra considering a 2° observer. The correlated color temperature value (CCT) of the white light was calculated using the empirical formula given by McCamy.[30] The photographs showing the luminescence of the phosphors deposited on Millipore filters were taken under illumination with ultraviolet radiation (λ = 254 nm) filtered from a Hg discharge lamp.

3. Results and discussion

3.1. Undoped $CaMoO_4$ particles

The effect of the GLY/H_2O ratio on the morphological characteristics of the particles precipitated by aging calcium nitrate (0.02 M) and sodium molybdate (0.1 M) solutions at 120°C for 20 h are summarized in Table 1 and Fig. 1. As observed, in pure glycerol

irregular and aggregated spheres were obtained (Fig. 1A). However, important differences in particle morphology and uniformity were found when adding H_2O to glycerol in variable GLY/H_2O volumetric ratios (Fig. 1B-E). Thus, uniform anisometric particles with similar size (about 3 μm x 1.3 μm) (Table 1) and different morphologies including peanuts (Fig. 1B), cocoons (Fig. 1C) and spindles (Fig. 1D) were obtained for a GLY/H_2O volumetric ratio of 4/1, 3.5/1.5 and 2.5:2.5, respectively. For a lower GLY/H_2O ratio (1.5/3.5 and pure water), more heterogeneous and aggregated particles resulted (Fig. 1E, F). Particle shape could be also modulated by using GLY/EG mixtures as solvent. Thus, uniform spheres (Fig. 2B) with a diameter of 1.2 μm (Table 1) resulted when a mixture of GLY/EG in a volumetric ratio of 2.5:2.5 was used as solvent, whereas irregular and aggregated entities were obtained when the GLY/EG ratio was varied (Fig. 2A, C) or in pure EG (Fig. 2D). Irrespective of morphology, the uniform precipitated particles were identified by XRD as tetragonal (scheelite-type) $CaMoO_4$ (ICDD file: 01-077-2238) as illustrated in Fig. 3 for the spheres, spindles and peanuts (cocoons will not be hereafter considered since this morphology is intermediate between peanuts and spindles).

A detailed observation of Fig. 1 and Fig. 2 also indicates that all homogeneous particles consisted of self-assembled much smaller crystals (Fig. 1B-D and 2B, inset). The size of such crystals estimated from the XRD patterns was found to be much lower for the spheres (34 nm) than for the other morphologies (96 nm for the peanuts and >100 nm, for the spindles) (Table 1). It should be noticed that the value of crystal size for the spindles is above the detection limit of the Scherrer formula (100 nm). However, the insets of Figures 1B and D clearly reveals the much higher size of the assembled crystals in the case of the spindles when compared to peanuts. This microstructure is characteristic of particles formed through an ordered aggregation process, similar to that

previously observed for different molybdates with scheelite structure.[22] Such mechanism was confirmed by analyzing the nature of the precipitates obtained after different aging times. Thus, in the case of the spindle-type particles, a high turbidity was detected after 1.5 min of aging, due to the precipitation of small and irregular particles (primary), which seem to aggregate to form larger spindles (Fig. 4A), which almost reached their final size after 5 min of aging (Fig. 4B). This process was accompanied by an increase of crystal size from 64 to >100 nm (Table 2), which seems to progress on prolonged aging from 5 min to 20 h, as observed by SEM (Fig. 4C). This behavior suggests that after aggregation, a recrystallization process also took place, since the reaction yield remained almost constant (~80%) during this period of aging (Table 2). A similar behavior was detected for the peanuts (Fig. 4D-F and Table 2) and the spherical particles (Fig. 4G-I and Table 2), except that the onset of precipitation was slightly slower in the first case and much slower for the latter, indicating that the reaction kinetics is faster as increasing the amount of water in the system. This result can be explained by taking into account the viscosity of the solvents (glycerol: 1.5 Pa·s, ethylene glycol: 0.01733 Pa·s, water: 0.001 Pa·s) since as increasing the amount of water, the viscosity of the solvent mixture decreases thus favoring the diffusion process required for nucleation and particle aggregation.

The different size and shape of the microarchitectures obtained using different solvents are difficult to explain since the particle formation through aggregation of primary particles is a very complex process involving many stages.[31] However, it is obvious that the primary particles must be brought together, which is a diffusion controlled step and therefore influenced by the viscosity of the solvent. Once the particles are close enough, the attractive interaction between them, whose driving force is the high surface energy of the small colloidal particles, must predominate over the

repulsive interparticle forces arising from their electric surface charge, whose magnitude is governed, among other factors, by acidity, ionic strength and dielectric constant of the solvent.[32] Therefore, the nature of the solvent determines the extent and pathway of aggregation between the interacting primary particles and hence, it must also greatly influence the morphological characteristics of the aggregates, which would justify, at least qualitatively, the morphological changes observed when using different solvents. Finally, it is outstanding the anisotropic morphology obtained in some cases (Fig. 1B-D). The formation of such a kind of non-spherical assemblies has been attributed to different causes, including the preferential aggregation of primary crystallites through their high energy facets to minimize surface energy[31] or the presence of adsorbed molecules on certain crystallographic plains, which are therefore unsuitable for aggregation. In our case, the later possibility cannot be discarded owing to the ability of the polyols molecules to adsorb on the surface of the precipitated particles.[33-36] In fact, the FTIR spectra recorded for all three morphologies (Fig. S1) displayed some weak bands in the 1040-1110, 1200-1450 and 2870-2930 cm^{-1} regions due to the presence of polyol molecules adsorbed on the particles surface, which are more intense in the case of the anisometric particles.

The luminescent properties of the uniform spheres, spindles and peanuts $CaMoO_4$ microarchitectures are shown in Fig. 5. As observed, irrespective of particle morphology, all samples showed similar excitation and emission spectra arising from a charge transfer process within the MoO_4^{2-} groups.[26] Thus, the excitation spectra consist of a broad band centered at 276 nm, whereas the emission spectra also displays a single broad band centered at 500 nm, which is responsible for the bluish-green emission observed for the samples on excitation with UV light (Fig. 5C). Finally, Fig. 5B also reveals that the emission intensity is higher for the spindles and lower for the spheres.

Such a differences in intensity may be associated with the different crystallite size of the samples which was higher for the spindles (crystal size > 100 nm) and lower (crystal size = 34 nm) for the spheres (Table 1). This interpretation would be in agreement with the previously reported increase in emission intensity observed on calcination of $CaMoO_4$ samples at high temperatures which resulted in an increase of the structural order.[37]

3.2. Ln-doped $CaMoO_4$ particles

For the preparation of Ln-doped $CaMoO_4$ phosphors, we first addressed the doping with Eu^{3+} cations as a proof of concept to analyze the effect of doping on the morphological and structural features of the obtained phosphors. For this purpose, the sample having the higher emission intensity (spindle-type particles) was first selected. It was found that for an Eu^{3+} doping level of 1% (Eu/Eu+Ca mol ratio), the morphology of the particles was preserved but their size distribution was much broader (Fig. S2A). This effect was even more pronounced when increasing the Eu content from 1 to 5% (Fig. S2B). In view of such size polydispersity, we proceeded to dope the particles with peanut morphology that also presented a stronger emission than spheres. In this case, the addition of 1% of Eu^{3+} resulted in uniform particles whose shape (Fig. S3A) and size (Table 3) were similar to those obtained for the undoped system (Fig. 1B and Table 1). For a higher Eu/(Eu+Ca) molar ratio (3%), a peanut morphology was still observed, although the size of precipitated particles was more heterogeneous (Fig. S3B). At higher doping levels (5%) much smaller and heterogeneous ellipsoidal particles were obtained (Fig. S3C).

The presence of Eu^{3+} in the uniform doped (1% Eu) peanut-like particles was confirmed by ICP analyses, which showed an experimental Eu/(Eu+Ca) ratio of 0.94%,

very similar to the nominal value (1%) (Table 3). XRD diffraction (Fig. S4) indicated that these doped particles also crystallized into the tetragonal $CaMoO_4$ phase. The unit cell parameters estimated form this XRD pattern were slightly higher than those corresponding to the undoped sample (Table 4) suggesting the incorporation of the Eu^{3+} cations into the $CaMoO_4$ crystalline structure. It is important to note the unit cell expansion observed on doping in spite of the smaller ionic radius of Eu^{3+} (1.066 Å) when compared with Ca^{2+} (1.120 Å). To explain this apparently anomalous behavior, it has to be kept in mind that the heteromorphic substitution of Ca^{2+} by Eu^{3+} requires charge compensation either by the introduction of Na^{+} (present in the reaction medium coming from the molybdate precursor),[24] by the generation of cationic vacancies[38] or by the introduction of interstitial oxygen.[38] Obviously, all these mechanisms should also influence the unit cell volume, which has been shown to increase in scheelite-type compounds only if cationic vacancies are present.[38] Nevertheless, the elucidation of the substitution mechanism operating in our case needs a deeper structural study which will be the subject of a forthcoming paper.

Finally, the formation of the Eu^{3+}:$CaMoO_4$ solid solution also affected crystallinity since the value of crystal size decreased (from 96 to 49 nm) as a consequence of the doping process (Table 4). This effect could be due to the ability of the doping cations to change the nucleation energy barriers as well as the nucleation and growth kinetics of nanocrystals.[39] Obviously, these changes in the crystal (and therefore, primary particles) size should have strong influence on the aggregation behavior, which would justify the changes in particle size and shape of the obtained doped microarchitectures.

The excitation spectra recorded for the Eu(1%)-$CaMoO_4$ phosphor with peanut shape monitored at 615 nm, which is the most intense Eu^{3+} emission band in this matrix,[13, 40] is presented in Fig. 6 (top). As observed, this spectrum displayed a strong broad band

centered at λ=276 nm, which is quite similar to that observed for the undoped samples and has been ascribed to the optical excitation of the molybdate anions followed by an energy transfer (ET) to the Eu^{3+} cations.[40]

Upon excitation within the ET band (λ_{ex}=276 nm), the characteristics transitions lines from the excited $^5D_0$ level to the ^7F_J (J=1, 2, 3, and 4) levels of the Eu^{3+} ions were detected (Fig. 6, bottom). It should be noticed that the most intense band, responsible of the re d luminescence of this sample (inset in Fig. 6, bottom), is that from the $^5D_0$-$^7F_2$ transition (615 nm), which indicates that the Eu^{3+} occupies a crystallographic site in the host lattice with no inversion center.[40] This behavior, which might seem surprising since the sites of the Ca^{2+} ions were the Eu^{3+} cation are located have inversion symmetry, indicates that the introduction of Eu^{3+} into the $CaMoO_4$ lattice induces a significant structural distortion as a consequence of the size an charge mismatch.[40]

In order to gain more information on the luminescent properties of this sample, the luminescent dynamics were also evaluated. The decay curve obtained for the $^5D_0 \rightarrow {}^7F_2$ Eu^{3+} transition of this sample (615 nm) could be fitted (Fig. 7A) by considering a bi-exponential decay:

$$I(t) = I_{01}\exp(-t/\tau_1)+I_{02}\exp(-t/\tau_2) \qquad (1)$$

where I(t) is the luminescence intensity, t is the time after excitation and τ_i *(i = 1, 2)* is the decay time of the *i*-component, with intial intensity I_{0i}. The fitting parameters are presented in Table 5, along with the average life-time values, <τ>, calculated as:

$$\langle\tau\rangle = \frac{\int_{t_0}^{t_f} tI(t)dt}{\int_{t_0}^{t_f} I(t)dt} = \left(\tau_1^2 I_1 + \tau_2^2 I_2\right)/\left(\tau_1 I_1 + \tau_2 I_2\right) \qquad (2)$$

where t_f represents the time required for the luminescence signal to reach the background. The biexponential decay observed for our sample is in agreement with previous reports on this phosphor,[13,21,40,41] according to which, the short component (τ = 390 ± 17 μs) is due to Eu^{3+} ions located close the nanoparticles surface and are influenced by OH-species or surface defects which act as luminescence quenchers,[42,43] whereas the long component (τ = 739 ± 37 μs) is ascribed to the Eu^{3+} ions located in the inner part of the particles, where surface effects are not present. It should be noted that the $<\tau>$ value obtained for our sample (600 ± 30 μs) is very close to the that reported for this kind of phosphor having the same Eu^{3+} content (662 μs).[40]

In order to develop a white light emitting phosphor, the peanut- like $CaMoO_4$ particles were doped with Dy^{3+} cations. In this case, particles with similar shape (Fig. S5A) and crystalline structure (Fig. S4) to those of the undoped system were also obtained for a doping level ≤1% Dy, although a slight decrease of particle size from 2.84 μm x 1.24 μm (Table 1) to 2 μm x 1 μm (Table 3) and crystallite size (from 96 to 77 nm) (Table 4) was noticed as in the case of Eu^{3+} doping. The successful incorporation of the Dy^{3+} cations into the $CaMoO_4$ particles was also confirmed by ICP analysis (Table 3) and by the unit cell expansion with respect to the undoped sample (Table 4).

The excitation spectrum obtained for the Dy(1%)-$CaMoO_4$ sample (Fig. 8A) by monitoring at a wavelength of 574 nm, which correspond to maximum of the emission band associated to the $^4F_{9/2}$ - $^6H_{13/2}$ transition of Dy^{3+} also displayed the strong and broad excitation band at λ=276 nm due to energy transfer process from the MoO_4^{2-} groups to the Dy^{3+} cations.[21] Upon exciting this sample at 276 nm (Fig. 8B), the characteristic emission bands of Dy^{3+} dominated the spectrum, which essentially consisted of two band groups in blue-green and yellow-orange region corresponding to the $^4F_{9/2}$ - $^6H_{15/2}$

and $^4F_{9/2}$ - $^6H_{13/2}$ electronic transitions of Dy^{3+}, respectively. It should be noted that the emission spectrum also displayed a broad (from 400 to 600 nm) and weak band in the bluish region due to the emission of $CaMoO_4$ matrix, indicating that the energy transfer process from the molybdate groups to the Dy^{3+} cations was not complete. The presence of this bluish band along with those of Dy^{3+} gave rise to a greenish light emission (Fig. 8C) whose chromatic coordinates (x = 0.297, y = 0.389) are close to the white light region of the CIE chromaticity diagram (Fig. 9). It should be noted that the color coordinates of some other reported Dy doped $CaMoO_4$ samples with the same doping level (x = 0.21, y = 0.35[44]; x = 0.22, y = 0.20[45]; x = 0.26, y = 0.257[21]) are even farther from the ideal white hue (x = 0.33, y = 0.33). As in the case of Eu^{3+} doping, the decay curve obtained for the $^4F_{9/2}$ - $^6H_{13/2}$ transition of Dy^{3+} (Fig. 7B), also showed a bi-exponential behavior (Table 5). The value of the average life-time $<\tau>$ (186 ± 9 μs) was also of the same order of magnitude as those previously reported (from 195[46] to 198[21] μs, for a Dy^{3+} content ranging from 2 to 4%).

As an attempt to achieve a whiter light emission from the Dy-doped sample, we varied the Dy doping level. As observed in Fig. 8B, the decrease of the Dy content from 1 to 0.35 % gave rise to a progressive increase of the relative intensity of the blue emission band due the molybdate matrix, which resulted in a decrease of the value of color coordinates (Table 6) involving a shift of the light hue from greenish to bluish (Fig. 9). This behavior resulted in an increase of the CCT from 6804 to 8253 K (Table 6). It should be noted that the greenish-blue hue observed for the Dy^{3+} single doped samples is due to lack of red component of the emission light. With the aim of obtaining a warmer light with coordinates closer to ideal white light (x = 0.333, y = 0.333), and therefore more appropriated for illumination purposes,[47] we proceeded to add a small amount of Eu^{3+} to the Dy^{3+} doped samples, which as shown above, emits red light under

excitation at the same wavelength than Dy^{3+} and the $CaMoO_4$ matrix. After different assays, we found that the emission spectrum of the $CaMoO_4$ particles codoped with a 0.35% Dy^{3+} and a 0.15% Eu^{3+} (Fig. 10) showed the bands due to Dy^{3+} and Eu^{3+} cations, as well as that of the $CaMoO_4$ matrix, with appropriated relative intensity so that a whiter (x = 0.335 and y = 0.365) (Fig. 9) and warmer (CCT = 5407 K) (Table 6) emission light was produced, which may be suitable for the development of LEDs for indoors illumination.[47] As expected, the addition of Eu^{3+} has no important effects on particle shape (Fig. S5B), size (Table 3) or crystalline structure (Fig. S4) of the $CaMoO_4$ based particles, although a decrease of crystallite size with respect to the undoped sample was also detected as observed for the single doped particles (Table 4).

Finally, the luminescence dynamics of the codoped sample were also evaluated to assess the possible existence of an energy transfer process between Dy^{3+} and Eu^{3+} in our white light emitting phosphor, which has been previously observed for other Eu^{3+}-Dy^{3+} codoped systems.[48] The decay curves obtained for the $^4F_{9/2}$-$^6H_{13/2}$ transition of Dy^{3+} (575 nm) and the $^5D_0$-$^7F_2$ transition of Eu^{3+} (615 nm) could be also fitted through a bi-exponential function (Fig. 7C, D) whose fitting parameters are shown in Table 5. As observed, the average life-time values, $<\tau>$ obtained for both Eu and Dy emissions, in the codoped sample were quite similar to those obtained for the single doped samples with the same doping level, indicating that no energy transfer between the doping cations takes place in the codoped sample and that the cooping process had no influence on the luminescence efficiency.

4. Conclusions

Uniform $CaMoO_4$ microarchitectures have been synthesized through precipitation reactions at 120 ºC from solutions containing calcium nitrate and sodium molybdate, using mixed solvents (polyols and water). The shape of such microarchitectures was found to be determined by the nature of the solvent mixture. Thus, peanuts, cocoons and spindles were obtained in glycerol-water mixtures with different polyol/water ratio, whereas spheres resulted in a ethylene glycol-water mixture. Irrespective of their shape, the obtained particles consisted of self-assembled nanocrystals which crystallized into the tetragonal $CaMoO_4$ phase. All these samples showed similar excitation and emission spectra arising from a charge transfer process within the MoO_4^{2-} groups. The emitted light presented a bluish-green color and its intensity was higher for the spindle-type particles, which might be associated to their higher crystallite size. This procedure was also suitable for doping the peanut like $CaMoO_4$ architectures with Eu^{3+} or Dy^{3+} cations up to a 1% molar ratio (Ln/Ln+Ca), without altering their morphology or crystalline structure. The so prepared phosphors emitted an intense red (Eu-doped) or greenish (Dy-doped) light when excited through the MoO_4^{2-} groups excitation band indicating the presence of an energy transfer process from such groups to the Ln^{3+} cations. Finally, a white light emitting phosphor with chromaticity coordinates x = 0.335 and y = 0.365, and a correlated color temperature of 5407 K was developed by cooping the peanut-type $CaMoO_4$ particles with proper amounts of Dy^{3+} (0.35%) and Eu^{3+} (0.15%) cations, which could find applications in white light emitting diodes.

Acknowledgements

This work has been supported by the Spanish Ministry of Economy and Competitiveness (MINECO) (MAT2014-54852-R) and CSIC (Pie 201460E005).

Table 1 Shape, size and crystallite size of the $CaMoO_4$ particles obtained at 120°C for 20 h from solutions containing calcium nitrate and sodium molybdate in different mixed solvents (polyols and water).

GLY/H_2O (vol)	GLY/EG (vol)	Shape	Larger dimension (μm)	Shorter dimension (μm)	Diameter (μm)	Crystallite size (nm)
5/0		Irregular sphere	-	-	-	-
4/1		Peanut	2.84(±0.23)	1.24(±0.09)	-	96
3.5/1.5		Cocoon	2.93(±0.26)	1.34(±0.1)	-	-
2.5/2.5		Spindle	2.78(±0.32)	1.29(±0.11)	-	>100
1.5/3.5		Irregular	Heterogeneous	Heterogeneous	-	-
0/5		Irregular	Heterogeneous	Heterogeneous	-	-
	2.5/2.5	Sphere	-	-	1.2(±0.15)	34

Table 2 Reaction yield and crystallite size for the samples with different particle shape obtained after different reaction times.

Shape	Time	Yield (%)	Crystallite size (nm)
Spindles	1.5 min	50	64
Spindles	5 min	82	>100
Spindles	20 hours	80	>100
Peanuts	3 min	82	25
Peanuts	5 min	91	38
Peanuts	20 horas	98	96
Spheres	2 hours	9.2	19
Spheres	4 hours	48	23
Spheres	20 hours	84	34

Table 3 Nominal and experimental (ICP) Ln/(Ln+Ca) mol ratio and sizes of the Ln-doped $CaMoO_4$ particles.

Ln/(Ln+Ca)		Larger dimension (μm)	Shorter dimension (μm)
Nominal (%)	ICP (%)		
1% Eu	0.89% Eu	2.45 (±0.42)	1.11 (±0.16)
1% Dy	1.07% Dy	2.1 (±0.1)	1.0 (±0.05)
0.35% Dy + 0.15% Eu	-	2.6 (±0.2)	1.3 (±0.1)

Table 4 Unit cell parameters, unit cell volumes and crystallite size measured for the Ln-doped $CaMoO_4$ particles with peanut morphology.

Ln content	a=b (Å)	c (Å)	V(Å^3)	Crystallite size (nm)
0% Eu	5.2268(2)	11.4424(5)	312.60	96
1% Eu	5.2273(2)	11.4467(7)	312.77	49
1% Dy	5.2273(2)	11.4439(6)	312.70	77
0.35% Dy + 0.15% Eu	5.2273(1)	11.4438(4)	312.70	69

Table 5 Lifetimes values (τ_1, τ_2) and average decay time ($< \tau >$) for the Ln-doped $CaMoO_4$ particles obtained for the $^5D_0$-$^7F_2$ transition of Eu^{3+} (615 nm) and the $^4F_{9/2}$-$^6H_{13/2}$ transition of Dy^{3+} (575 nm) after pulsed excitation with λ_{exc} 532 and 355 nm respectively, as a function of the Ln content.

Emission	Eu content (%)	Dy content (%)	I_1	τ_1 (μs)	I_2	τ_2 (μs)	$< \tau >$ (μs)
Eu (615 nm)	1%	-	0.647	390 ± 17	0.515	739 ± 37	600 ± 30
Eu (615 nm)	0.15%	-	0.451	330 ± 20	0.712	739 ± 37	649 ± 32
Eu (615 nm)	0.15%	0.35%	0.480	340 ± 17	0.662	739 ± 37	639 ± 32
Dy (575 nm)	-	1%	0.385	26 ± 1.3	0.572	200 ± 10	186 ± 9
Dy (575 nm)	-	0.35%	0.245	26 ± 1.3	0.704	200 ± 10	192 ± 10
Dy (575 nm)	0.15%	0.35%	0.286	26 ± 1.3	0.640	200 ± 10	190 ± 10

Table 6 CIE color coordinates (x, y) and correlated color temperature (CCT) value corresponding to the emissions of the single Dy-doped and Dy-Eu bidoped $CaMoO_4$ samples.

Sample	x	y	CCT (K)
1% Dy	0.297	0.389	6804
0,7% Dy	0.285	0.384	7345
0,5% Dy	0.276	0.378	7821
0,35% Dy	0.269	0.372	8253
0,35%Dy + 0,15%Eu	0.335	0.365	5407

References

1 J.C.G. Bünzli and C. Piguet, *Chem. Soc. Rev.*, 2005, **34**, 1048.

2 X. Zhai, S. Liu, X. Liu, F. Wang, D. Zhang, G. Qin and W. Qin, *J. Mater. Chem. C*, 2013, **1**, 1525.

3 R. P. Rao and D. J. Devine, *J. Lumin*, 2000, **87-89**, 1260.

4 M. Shang, C. Li and J. Lin, *Chem. Soc. Rev.*, 2014, **43**, 1372.

5 W. Yang, X. Li, D. Chi, H. Zhang and X. Liu, *Nanotech*, 2014, **25**, 482001.

6 W. Zheng, D. Tu, P. Huang, S. Zhou, Z. Chen and X. Chen, *Chem. Commun.*, 2015, **51**, 4129.

7 H. Dong, S. R. Du, X. Y. Zheng, G. M. Lyu, L. D. Sun, L. D. Li, P. Z. Zhang, C. Zhang and C. H. Yan, *Chem. Rev.*, 2015, **115**, 10725.

8 Z. Chen, W. Zheng, P. Huang, D. Tu, S. Zhou, M. Huang and X. Chen, *Nanoscale*, 2015, **7**, 4274.

9 G. Blasse, *Mater. Chem. Phys.*, 1987, **16**, 201.

10 K. G. Sharma and N. R. Singh, *New J. Chem.*, 2013, **37**, 2784.

11 A. M. Kaczmarek and R. V. Deun, *Chem. Soc. Rev.*, 2013, **42**, 8835.

12 F. Lei and B. Yan, *J. Solid State Chem.*, 2008, **181**, 855.

13 Z. Hou, R. Chai, M. Zhang, C. Zhang, P. Chong, Z. Xu, G. Li and J. Lin, *Langmuir*, 2009, **25**, 12340.

14 J. H. Chung, J. H. Ryu, S. W. Mhin, K. M. Kim and K. B. Shim, *J. Mater. Chem.*, 2012, **22**, 3997.

15 A. Kuzmanoski, V. Pankratov and C. Feldmann, *Solid State Sci.*, 2015, **41**, 56.

16 L. Yang, G. Li, M. Zhao, J. Zheng, D. Luo, Y. Zheng and L. Li, *Eur. J. Inorg. Chem.*, 2013, 5999.

17 J. Huang, H. Luo, P. Zhou, X. Yu and Y. Li, *J. Lumin.*, 2007, **126**, 881.

18 A. I. Prasad, A. K. Parchur, R. R. Juluri, N. Jadhav, B. N. Pandey, R. S. Ningthoujam and R. K. Vatsa, *Dalton Trans.*, 2013, **42**, 4885.

19 C. Hazra, T. Samanta, A. V. Asaithambi and V. Mahalingam, *Dalton Trans.*, 2014, **43**, 6623.

20 Y. Sun, C. Li, Z. Zhang, X. Ma, L. Wang, Y. Wang, M. Song, P. Ma, L. Jiang and Y. Guo, *Solid State Sci.*, 2012, **14**, 219.

21 L. Li, R. Li, W. Zi and S. Gan, *Phys. B*, 2015, **458**, 8.

22 V. M. Longo, L. S. Cavalcante, E. C. Paris, J. C. Sczancoski, P. S. Pizani, M. S. Li, J. Andres, E. Longo and J. A. Varela, *J. Phys, Chem. C*, 2011, **115**, 5207.

23 D. Chen, K. Tang, F. Li and H. Zheng, *Cryst. Growth Des.*, 2006, **6**, 247.

24 X. Liu, L. Li, H. M. Noh, J. H. Jeong, K. Jang and D. S. Shin, *RSC Adv.*, 2015, **5**, 9441.

25 V. S. Marques, L. S. Cavalcante, J. C. Sczancoski, A. F. P. Alcantara, M. O. Orlandi, E. Moraes, E. Longo, J. A. Varela, L. M. Siu and M. R. M. C. Santos, *Cryst. Growth Des.*, 2010, **11**, 4752.

26 G. S. R. Raju, E. Pavitra, Y. H. Ko and J. S. Yu, *J. Mater. Chem.*, 2012, **22**, 15562.

27 F. Yu, J. Zuo, Z. Zhao, C. Jiang and Q. Yang, *Mater. Res. Bull*. 2011, **46**, 1327.

28 Y. Liu, G. Liu, J. Wang, X. Dong and W. Yu, *Inorg. Chem.*, 2014, **53**, 11456.

29 S. G. Lee, Y. J. Kim, S. J. Yoo, S. H. Lee and J. G. Kim, *JAST,* 2012, **3**, 128.

30 C. S. McCamy, *Color Res. Appl.*, 1992, **2**, 142.

31 Z. Wu, S. Yang and W. Wu, *Nanoscale*, 2016, **8**, 1237.

32 P. C. Hiemenz and R. Rajagopalan, *Principles of Colloid and Surface chemistry*, 3rd ed., rev. and expanded, Marcel Dekker, Inc 1997, ISBN 0-8247-9397-8.

33 X. Wang, J. Zhuang, Q. Peng and Y. Li, *Nature***,** 2005, **437/1**, 121.

34 Z. L. Wang, Z. W. Quan, P. Y. Jia, C. K. Lin, Y. Luo, Y. Chen, J. Fang, W. Zhou, C. J. O'Conor and J. Lin, *Chem. Mater.*, 2006, **18**, 2030.

35 Y. Wei, F. Lu, X. Zhang and D. Chen, *Mater. Lett.*, 2007, **61**, 1337.

36 N. O. Nuñez and M. Ocaña, *Nanotechnology*, 2007, **18**, 455606.

37 V. M. Longo, A. T. Figueiredo, A. B. Campos, J. W. M. Espinosa, A. C. Hermandes, C. A. Taft, J. R. Sambrano, J. A. Varela and E. Longo, *J. Phys. Chem. A*, 2008, **112**, 8920.

38 P. Jiang, W. Gao, R. Cong and T. Yang, *Dalton Trans.*, 2015, **44**, 6175.

39 D. Chen and Y. Wang, *Nanoscale*, 2013, **5**, 4621.

40 S. K. Gupta, M. Sahu, P. S. Ghosh, D. Tyagi, M. K. Saxena and R. M. Kadama, *Dalton Trans.*, 2015, **44**, 18957.

41 M. Li, F. Liu, J. P. Cheng, J. Ying and X. B. Zhang, *J. Alloys & Compounds*, 2015, **635**, 225.

42 A. I. Becerro, S. Rodríguez-Liviano, A. J. Fernández-Carrión and M. Ocaña, *Cryst. Growth Des.*, 2013, **13**, 526.

43 F. N. Sayed, V. Grover, V. Sudarsan, B. N. Pandey, A. Asthana, R. K. Vatsa and A. K. Tyagi, *J. Colloid Interface Sci.*, 2012, **367**, 161.

44 S. K. Sharma, S. Dutta, S. Som and P. S. Mandal, *J. Mater. Sci. Technol*., 2013, **29(7)**, 633.

45 S. Dutta, S. Som and S. K. Sharma, *Dalton Trans.*, 2013, **42**, 9654.

46 K. G. Sharma and N. R. Singh, *New J. Chem.*, 2013, **37**, 2784.

47 Li, J. D. Budai, F. Liu, J. Y. Howe, J. Zhang, X. J. Wang, Z. Gu, C. Sun, R. S. Meltzer and Z. Pan, *Light: Science and Application*, 2013, **2**, e50, doi:10.1038/Isa.2013.6.

48 H. Guan, G. Liu, J. Wang, X. Dong and W. Yu, *New J. Chem.,*2014, **38**, 4901.

Figures

Fig. 1 SEM images of the particles obtained by aging at 120°C for 20 h, solutions containing $Ca(NO_3)_2$ (0.02 mol dm^{-3}) and Na_2MoO_4 (0.1 mol dm^{-3}) and using different solvents: A) pure glycerol (GLY), B) GLY/H_2O = 4/1; C) GLY/H_2O = 3.5/1.5; D) GLY/H_2O = 2.5:2.5; E) GLY/H_2O = 1.5/3.5; F) pure water.

Fig. 2 SEM (A and B) and TEM (C and D) images of the particles obtained by aging at 120°C for 20 h, solutions containing $Ca(NO_3)_2$ (0.02 mol dm^{-3}) and Na_2MoO_4 (0.1 mol dm^{-3}), using GLY/EG mixtures as solvent: A) GLY/EG = 3.5/1.5; B) GLY/EG = 2.5/2.5; C) GLY/EG = 2/3; D) pure ethylene glycol (EG).

Fig. 3 X-ray diffraction patterns obtained for the particles shown in Fig. 1D (spindles), 1B (peanuts) and 2B (spheres). The PDF file for tetragonal $CaMoO_4$ is also included.

Fig. 4 SEM images of the particles obtained by aging at 120°C for different reaction time, solutions containing $Ca(NO_3)_2$ (0.02 mol dm^{-3}) and Na_2MoO_4 (0.1 mol dm^{-3}) using different solvents: A-C) GLY/H_2O = 2.5/2.5; D-F) GLY/H_2O = 4/1 and G-I) GLY/EG = 2.5/2.5.

Fig. 5 (A) Excitation spectra (λ_{em}= 500 nm) and (B) emission spectra (λ_{ex}= 276 nm) recorded for the $CaMoO_4$ particles having different morphologies. (C) Color resulting from the emission of the different samples under excitation with UV light (λ = 312 nm).

Fig. 6 Excitation (λ_{em}= 615 nm) (top) and emission (λ_{ex}= 276 nm) (bottom) spectra recorded for the Eu(1%):$CaMoO_4$ particles having peanut-like morphology. Inset: Color of the emission for the Eu-doped particles under UV illumination (λ = 312 nm).

Fig. 7 Photoluminescence decay profile obtained for the most intense emission of the $CaMoO_4$ particles doped: (A) single doped with 1% of Eu, (B) single doped with1% of Dy, (C) single doped with 0.15% of Eu and codoped with 0.35% Dy + 0.15% Eu and (D) single doped with 0.35% of Dy and codoped with 0.35% Dy + 0.15% Eu.

Fig. 8 (A) Excitation spectrum (λ_{em}= 574 nm) recorded for the Dy(1%):$CaMoO_4$ peanut-like particles, (B) Normalized emission spectra (λ_{ex}= 276 nm) recorded for the peanut-like particles doped with different amounts of Dy and (C) Color of the emission for the Dy-doped particles with different doping levels under UV (λ = 312 nm) irradiation.

Fig. 9 CIE diagram showing the chromatic coordinates of the $CaMoO_4$ particles single doped with different Dy content (0.35-1%) and codoped with 0.35% Dy + 0.15% Eu.

Fig. 10 Emission spectrum (λ_{ex}= 276 nm) recorded for the $CaMoO_4$ particles codoped with 0.35% Dy + 0.15% Eu. Inset: Color of the emission of the codoped particles under UV illumination (λ = 312 nm).

Table of Contents

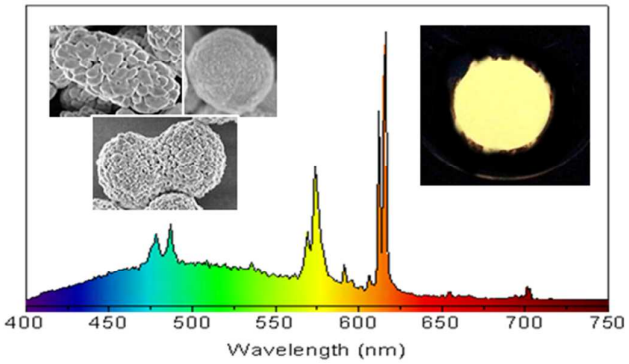

Uniform Eu^{3+},Dy^{3+}:$CaMoO_4$ microarchitectures fabricated in polyol media: morphology control through solvent selection and tunable photoluminescence through adjustment of doping levels.

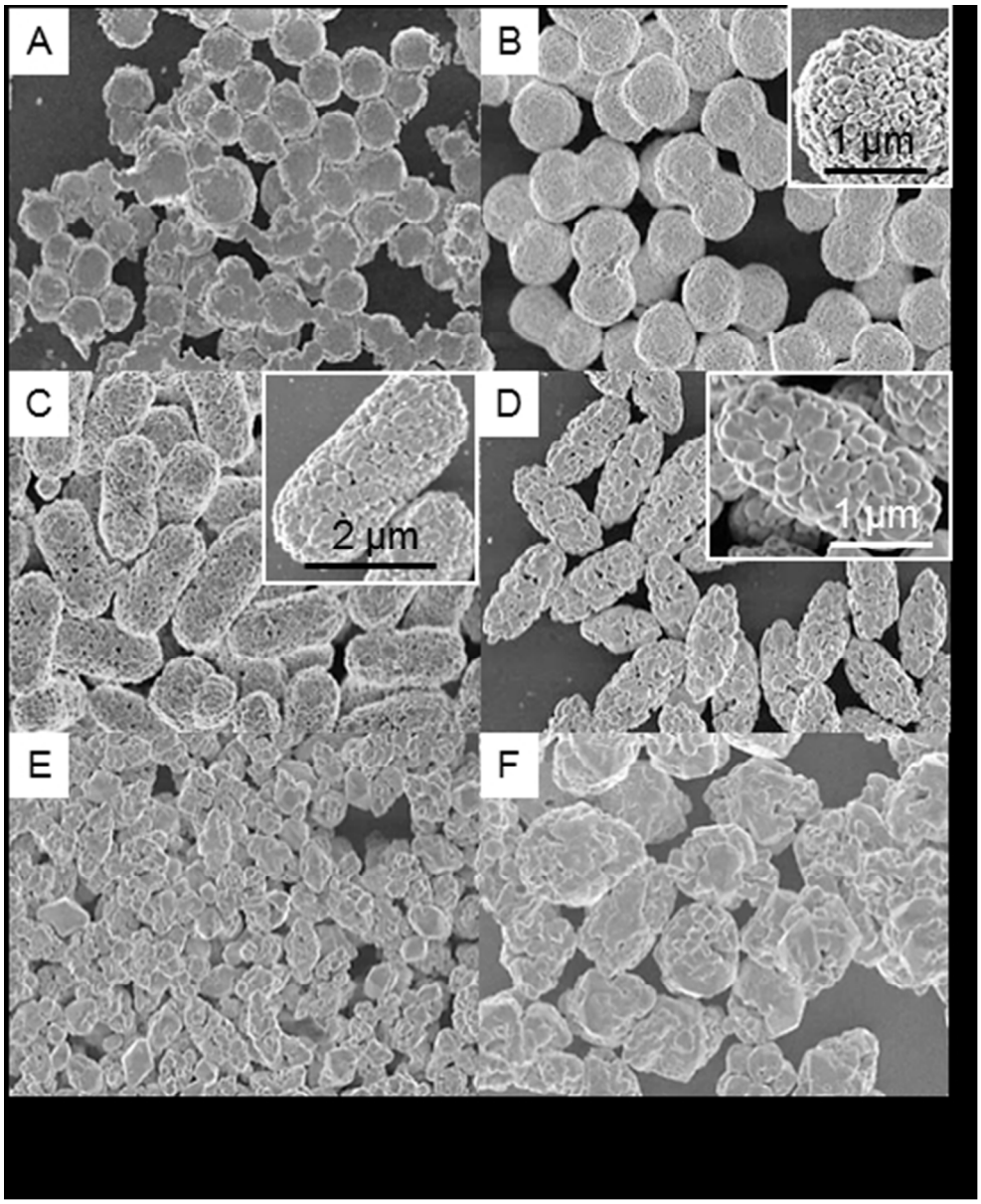

Fig. 1

82x101mm (150 x 150 DPI)

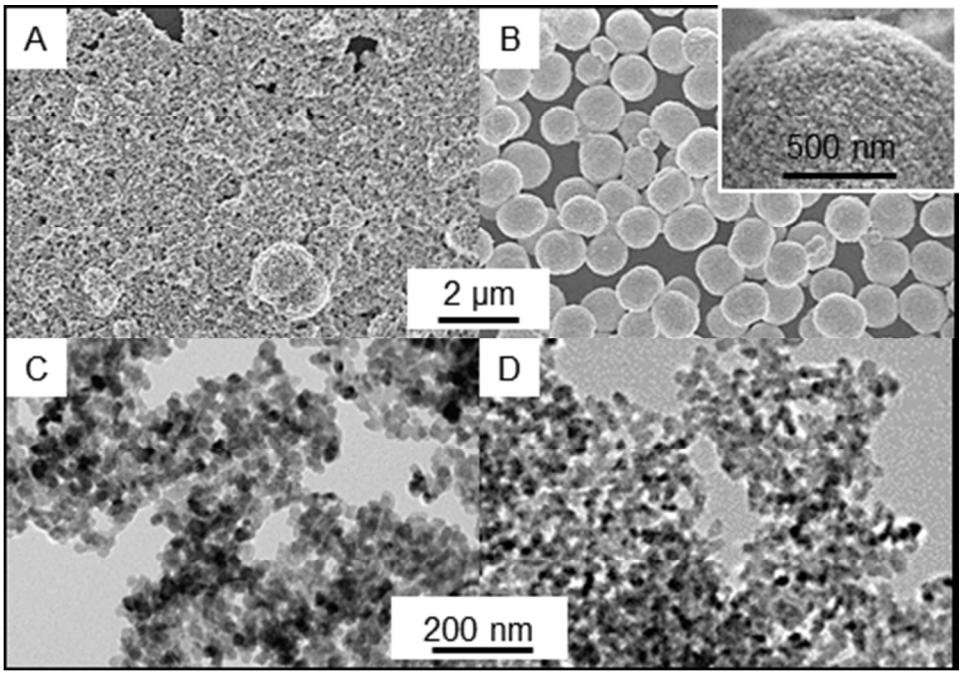

Fig. 2

80x56mm (150 x 150 DPI)

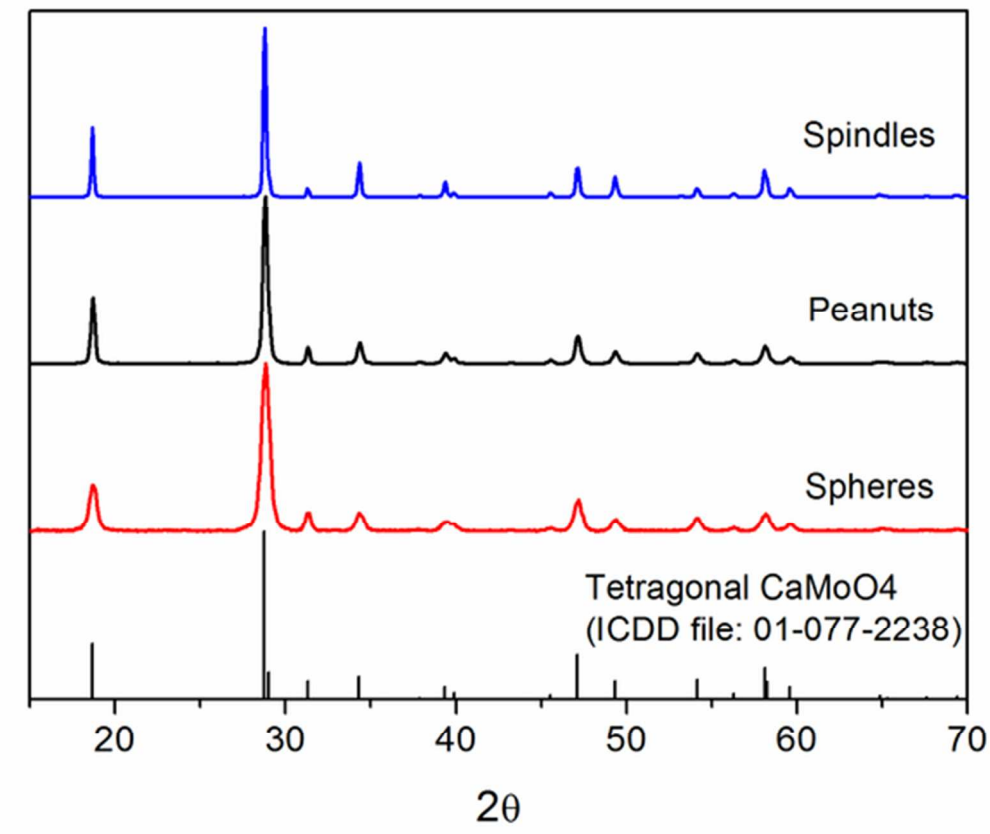

Fig. 3

48x41mm (300 x 300 DPI)

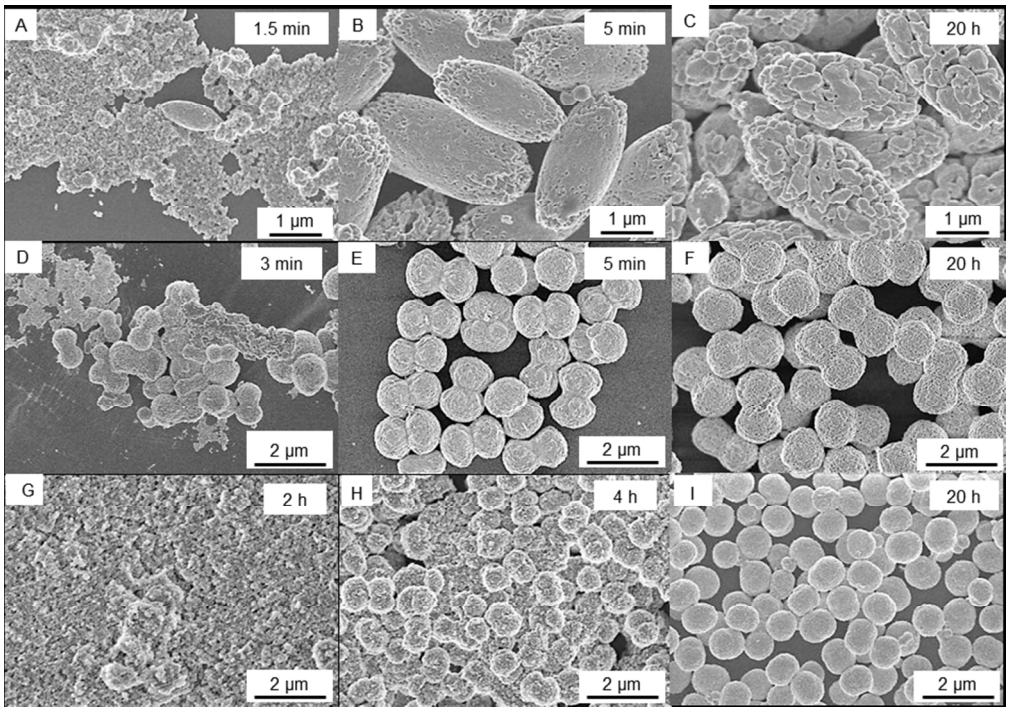

Fig. 4

159x111mm (150 x 150 DPI)

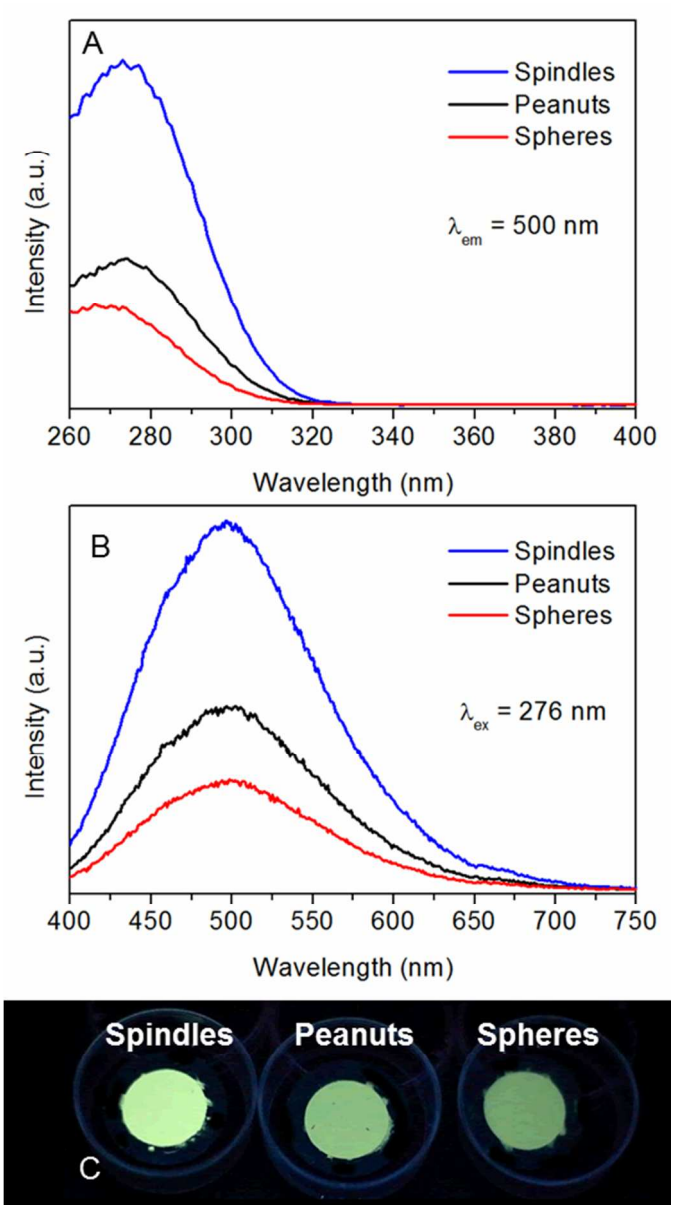

Fig. 5

90x163mm (150 x 150 DPI)

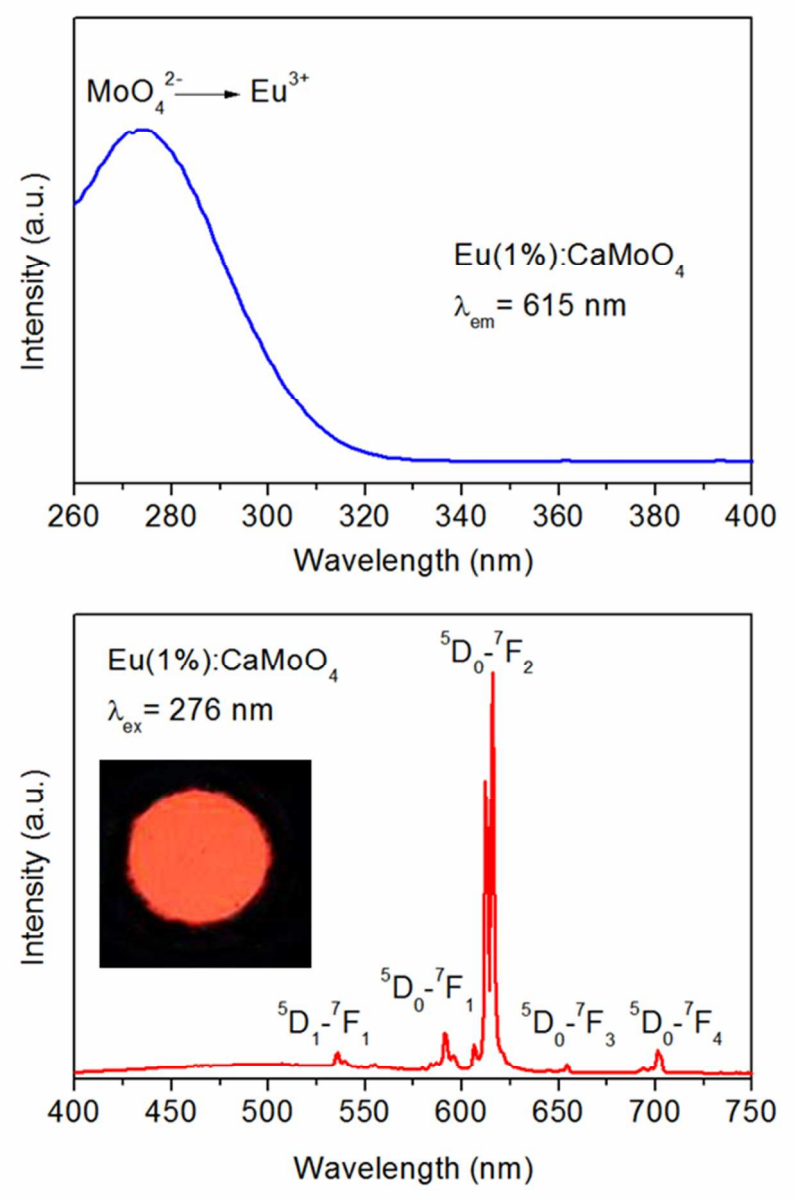

Fig. 6

96x144mm (150 x 150 DPI)

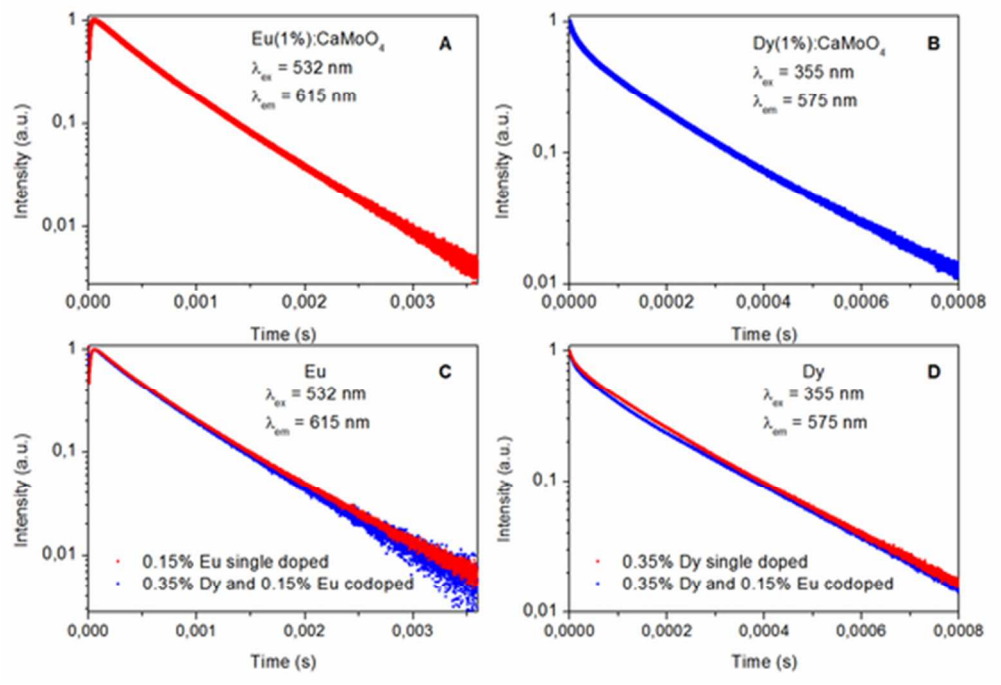

Fig. 7

45x31mm (300 x 300 DPI)

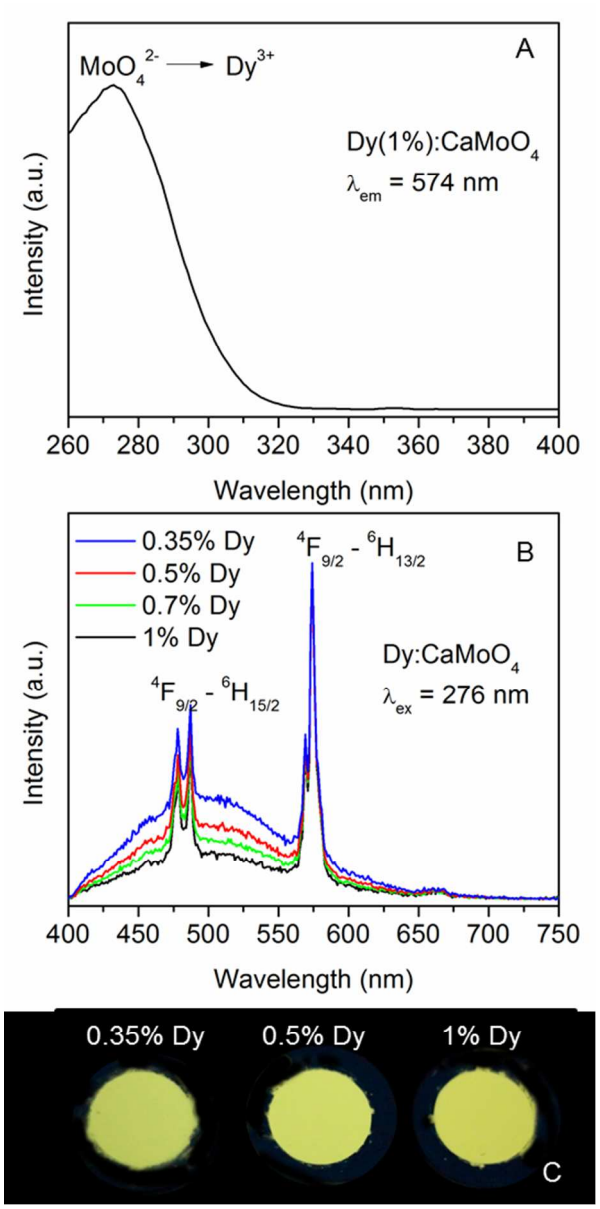

Fig. 8

91x185mm (150 x 150 DPI)

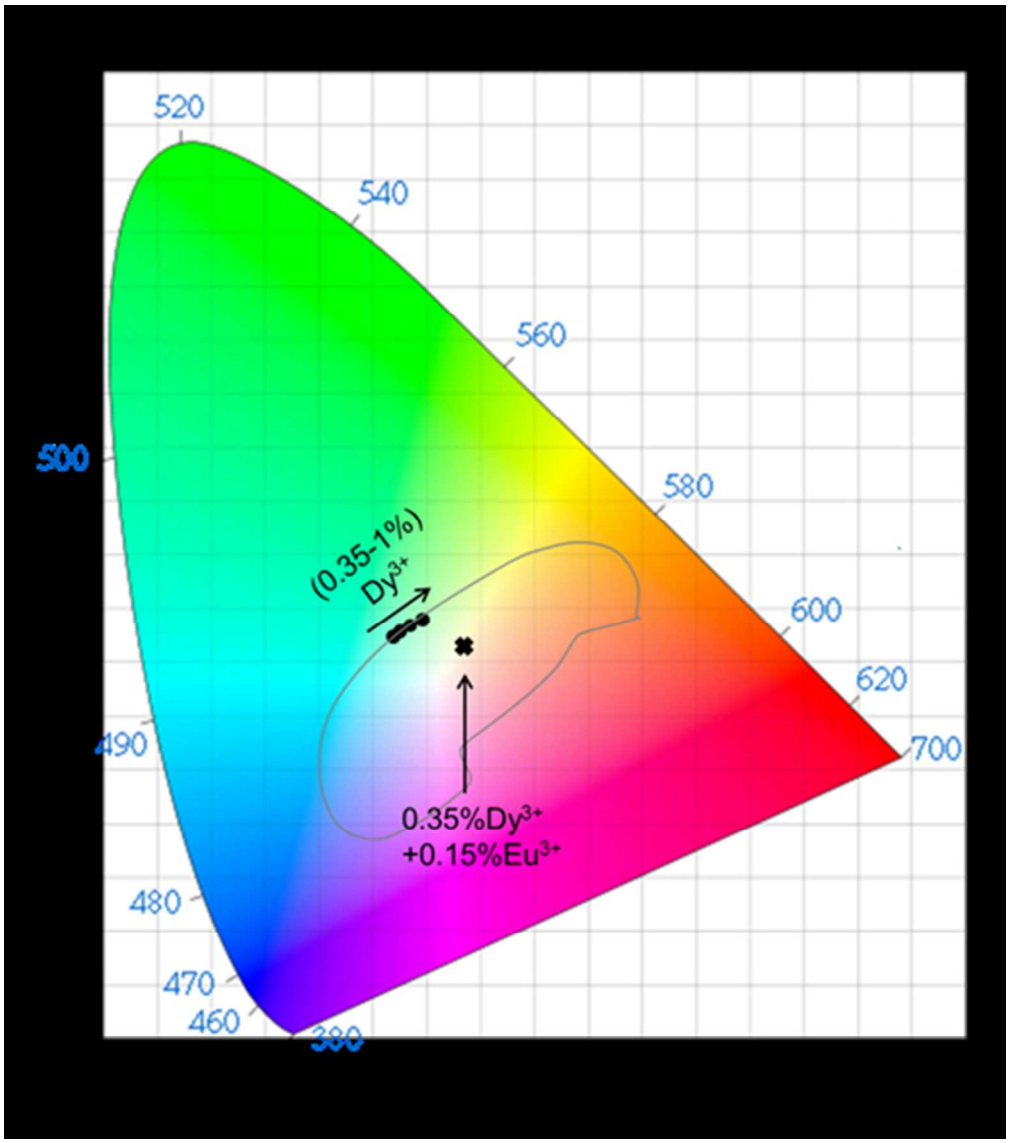

Fig. 9

87x98mm (150 x 150 DPI)

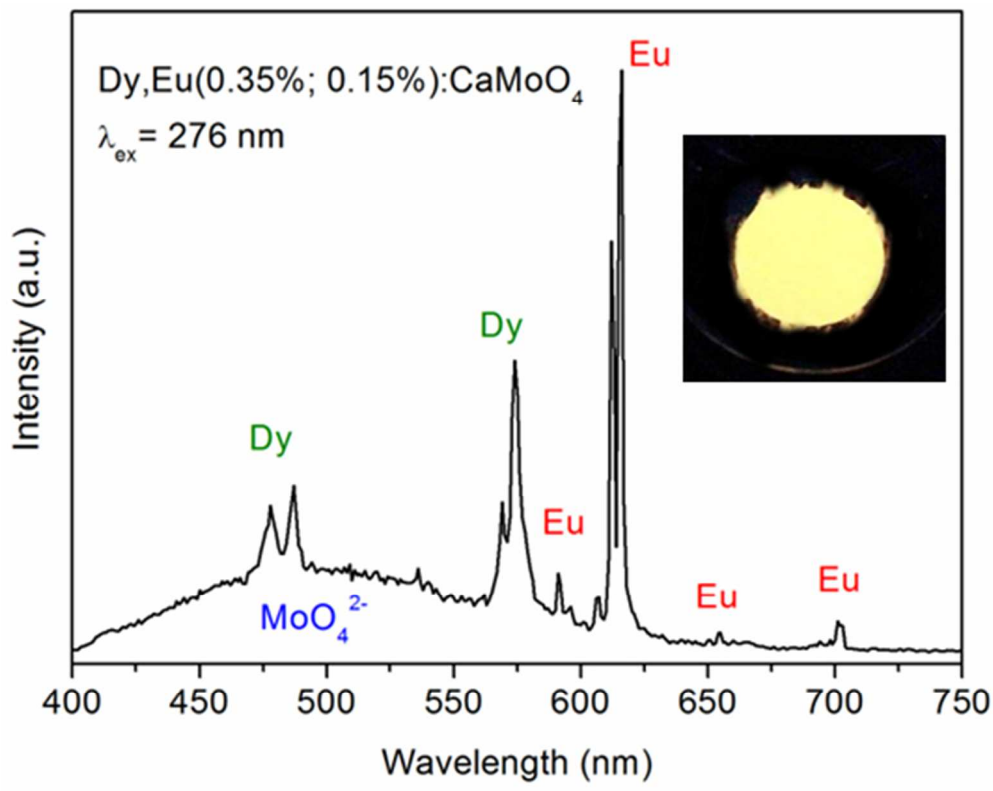

Fig. 10

90x71mm (150 x 150 DPI)

Electronic Supplementary Information

Morphology control of uniform $CaMoO_4$ based self-assembled microarchitectures and development of white light emitting phosphors by Ln doping (Ln= Dy^{3+}, Eu^{3+})

Mariano Laguna, Nuria O. Nuñez,* Ana I Becerro and Manuel Ocaña

Instituto de Ciencia de Materiales de Sevilla, CSIC, Américo Vespucio 49, 41092, Isla de la Cartuja, Sevilla, Spain

* corresponding author: nurianu@icmse.csic.es

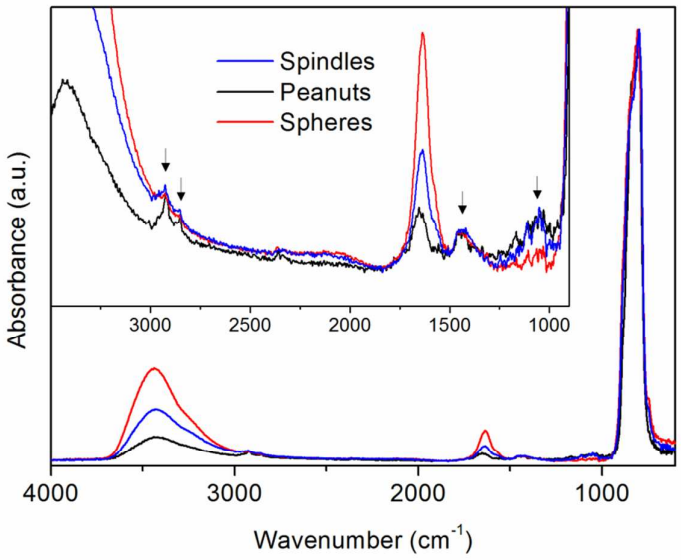

Fig S1 FTIR spectra for the $CaMoO_4$ samples with different morphology. Inset: bands mark with arrows can be ascribed to the presence of polyol (ethylene glycol and/or glycerol) molecules adsorbed on the particles surface. The spectra of the pure ethylene glycol (EG) and glycerol (GLY) can be found at:

EG: http://webbook.nist.gov/cgi/cbook.cgi?ID=C107211&Units=SI&Type=IR SPEC&Index=1#IR-SPEC

GLY: http://webbook.nist.gov/cgi/cbook.cgi?ID=C56815&Units=SI&Type=IR-SPEC&Index=1#IR-SPEC

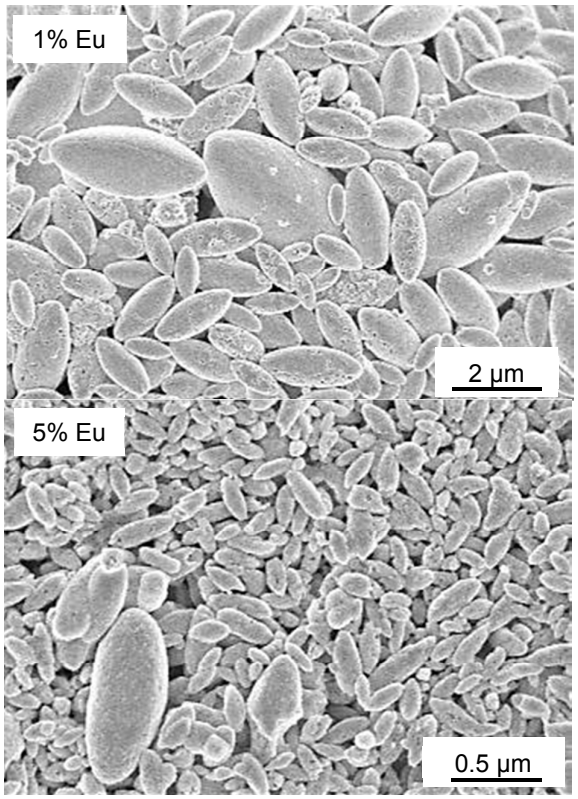

Fig S2 SEM images of the spindle-type $CaMoO_4$ particles with different Eu^{3+} doping level (Eu/Eu+Ca mol ratio).

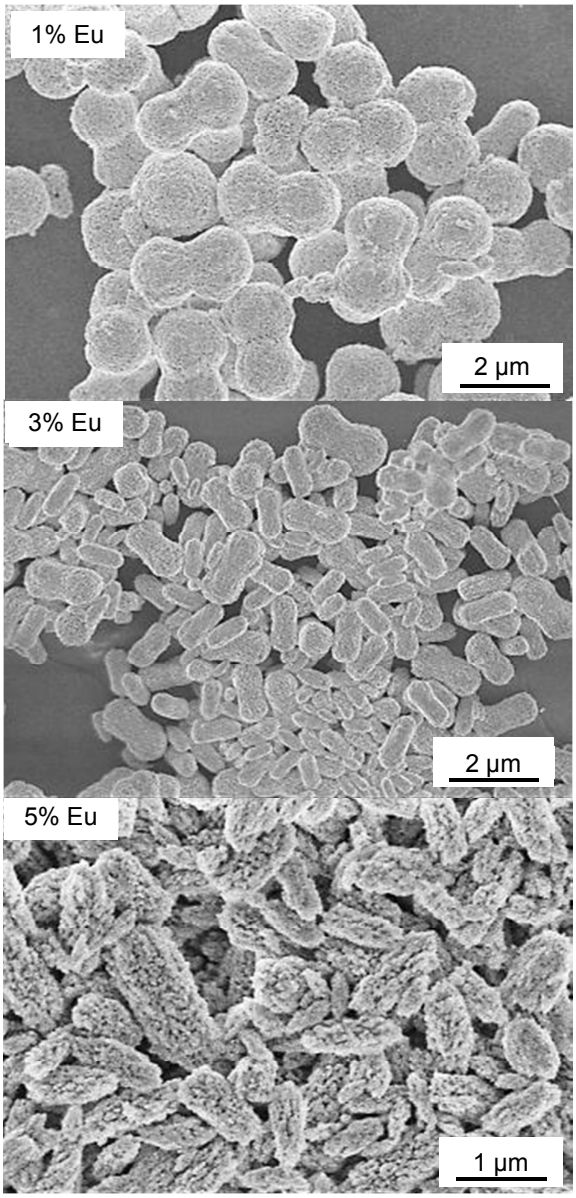

Fig S3 SEM images of the peanuts-type $CaMoO_4$ particles having different Eu content (Eu/Eu+Ca mol ratio).

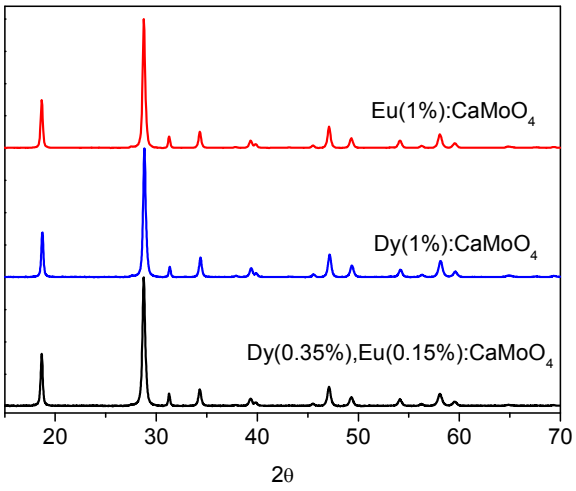

Fig S4 X-ray diffraction patterns obtained for the peanuts-type $CaMoO_4$ particles doped with 1% of Eu, 1% of Dy and codoped with 0.35% Dy + 0.15% Eu (Ln/Ln+Ca mol ratio).

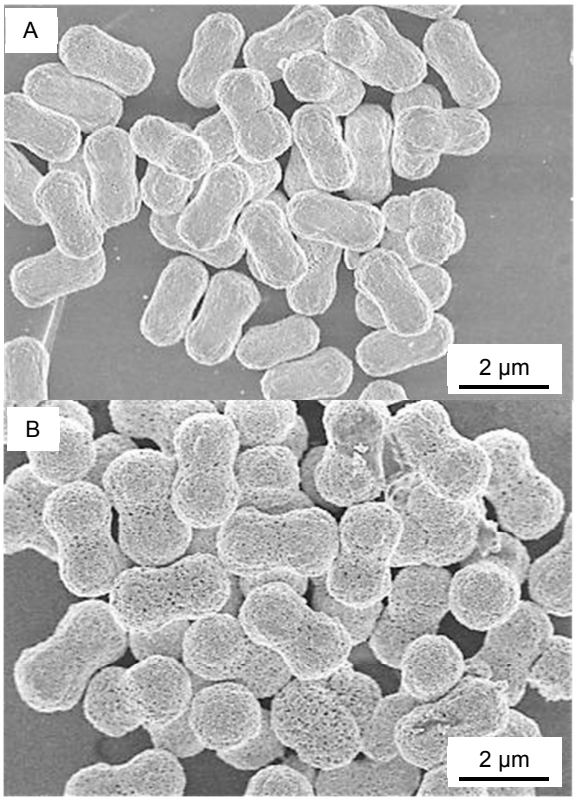

Fig S5 SEM images of the peanuts-type $CaMoO_4$ particles doped with 1% of Dy (A) and codoped with 0.35% Dy + 0.15% Eu (B).

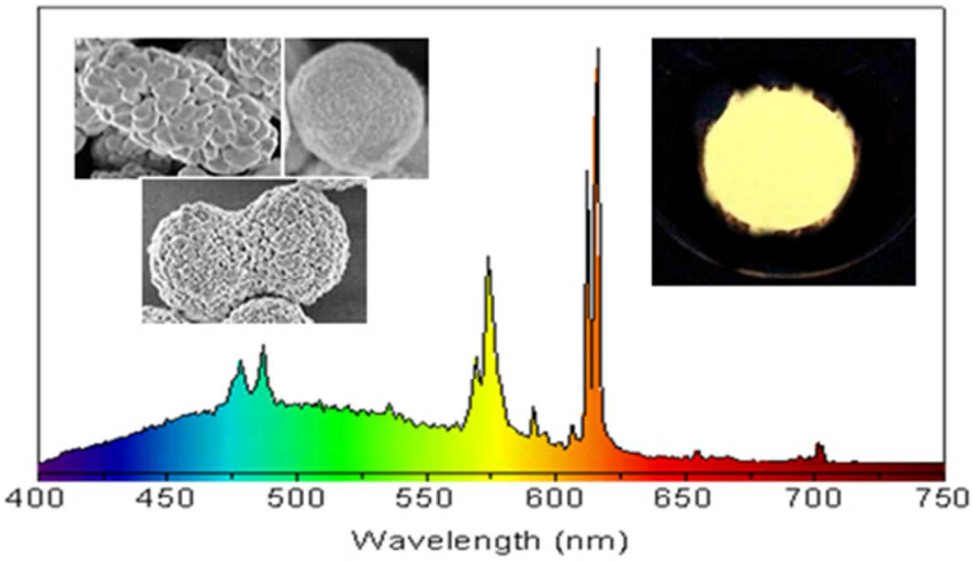

90x54mm (150 x 150 DPI)